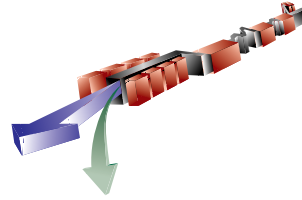


# 9

## X-Ray Beam Transport and Diagnostics



---

---

### *TECHNICAL SYNOPSIS*

*The photon beam transport system will deliver the LCLS radiation to the experiments. It is scientifically desirable to perform certain types of experiments relatively close to the x-ray source (the undulator), while others are better carried out at a distance of several hundred meters from the source. Therefore a long beamline is planned, with experimental areas grouped in two experimental halls, beginning about 50 m and about 400 m from the source. The beamline passing from the source through these halls will transport the FEL beam in high vacuum to the experimental apparatus. Several experimental stations will be built in these halls, and there is room for future expansion. However, only one experiment will be active at a time, and beam stops will be inserted to shield the areas downstream from the active experiment.*

*The x-ray optics system has the job of filtering the intensity, spectral, and spatial characteristics of the FEL beam as needed for the experiments. Most of the techniques that will be applied to perform the filtering (slits, absorbers, mirrors, monochromators) are commonly used at synchrotron sources. However, the LCLS presents special concerns due to the very high peak power density in the FEL beam. The LCLS optics system has been conservatively designed to perform under conditions of extreme peak power. An experimental program for studying high-power effects is planned.*

*The beam transport and optics systems will be used together to enable an extensive array of diagnostics measurements on the FEL x-ray pulses. The diagnostics instruments will be used to characterize the FEL beam during the initial commissioning of LCLS, and also to monitor the performance of LCLS during experimental operation.*

---

---

## **9.1 Introduction**

### **9.1.1 Objectives**

The x-ray beam transport system comprises the photon beamline components between the undulator and the User experiments. The design is based on the User and FEL physics requirements for the x-ray optics and x-ray diagnostics, as well as the facility requirements (i.e., the facility protocols and guidelines). The User and FEL physics requirements are discussed in Chapter 3.

The chapter begins with a presentation of general considerations for the design of optical elements and beam transport. **Section 9.2** then gives a detailed discussion of the beamline layout and the optical components included. **Section 9.3** describes the mechanical support and vacuum

techniques to be used throughout the beamline. **Section 9.4** presents the plans for beam diagnostics that will be used for initial studies of the FEL process, and for beam characterization during User experiments.

## 9.1.2 General Considerations

### 9.1.2.1 Beam Characteristics

In translating the User and facility requirements to hardware, the attributes of the FEL x-ray output must be considered. Detailed properties of both the coherent and spontaneous radiation have been calculated. The characteristics, that are most relevant for the beam transport and optics design (including power density on the optical elements), are shown in **Table 9.1** for locations approximating the front of Hall A, and Hall B.

**Table 9.1** Characteristics of the FEL x-ray beam

| FEL photon energy   | 0.828 keV (4.54 GeV electrons) |                      | 8.27 keV (14.35 GeV electrons) |                      |
|---|--------------------------------|----------------------|--------------------------------|----------------------|
|   | FEL fundamental                | Spontaneous          | FEL fundamental                | Spontaneous          |
| Energy per pulse (mJ)   | 3                              | 1.4                  | 2.5                            | 22                   |
| Peak power (GW)   | 11                             | 4.9                  | 9                              | 81                   |
| Photons/pulse   | $23 \times 10^{12}$            |                      | $1.9 \times 10^{12}$           |                      |
| Divergence ( $\mu$ rad FWHM)                                  | 9                              | 780                  | 1                              | 250                  |
| Spot size at 50 m<br>Hall A ( $\mu$ m FWHM)                   | 610                            | Limited by apertures | 130                            | Limited by apertures |
| Spot size at 400 m<br>Hall B ( $\mu$ m FWHM)                  | 4400                           |                      | 570                            |                      |
| Peak energy density at 50 m<br>Hall A ( $J\text{ cm}^{-2}$ )  | 0.59                           |                      | 11.9                           |                      |
| Peak energy density at 400 m<br>Hall B ( $J\text{ cm}^{-2}$ ) | 0.01                           |                      | 0.57                           |                      |

Due to its comparatively large divergence, most of the spontaneous radiation will intersect the walls of the undulator beam pipe or the first fixed mask of the optical system, and will not be transmitted into the experimental Halls. The on-axis spontaneous radiation that will reach the Halls consists mostly of odd harmonics of the undulator fundamental, with a spectral flux about five orders of magnitude below that of the FEL fundamental [1].

One of the principal design goals of the LCLS optics system is to contain the main photon beam entirely within the beamline vacuum pipe under all conditions. Because of its small divergence, this goal is not difficult to achieve without limiting the passage of the FEL beam. The spontaneous radiation must be limited, and this will be achieved by placing apertures (fixed masks) at the entrance points of the experimental Halls.

### 9.1.2.2 Photon-Induced Damage

Only the coherent light poses a problem; the spontaneous emission is divergent and will be reduced by upstream apertures. The spontaneous radiation is also mostly at larger energies than the fundamental, and is not strongly absorbed in optical components.

#### *Normal Incidence*

A material exposed to the LCLS FEL radiation at normal incidence will experience an unprecedented peak x-ray power density. X-ray absorption and damage mechanisms under these conditions have never been explored experimentally, and may exhibit nonlinear effects. One of the goals of initial LCLS research will be to study these effects. However, the nonlinear effects are expected to be much weaker than those encountered in the visible region of the spectrum [2]. Therefore, for the purpose of estimating damage to optical materials, it is not unreasonable to use linear extrapolations of known absorption and melting properties. **Table 9.2** shows linear-extrapolation calculations for different materials at the location of Hutch A2, near the front of experimental hall A, for the worst case FEL energy of 827 eV where absorption is largest, and also for an energy of 8270 eV [3]. Dose rates given here are for normal incidence, calculated from photo-ionization cross sections, with the photon beam areal density calculated for a propagated Gaussian beam.

Comparing the predicted dose and the dose required to melt, one finds that Li, Be, and possibly B and C can be safely used in the unattenuated FEL beam at the location of Hutch A2 throughout the energy range of LCLS (although these latter materials approach 0.5 of the melt limit at the low-energy end of the range). At the higher energies, Si can possibly be used also.

**Table 9.2** Normal-incidence peak energy dose and damage to materials in Hutch A2.

| Material     | Melt (eV/atom) | Dose (eV/atom) |         |
|--------------|----------------|----------------|---------|
|              |                | 827 eV         | 8270 eV |
| Li           | 0.1            | 0.02           | 0.0005  |
| Be           | 0.3            | 0.08           | 0.001   |
| B            | 0.5            | 0.2            | 0.003   |
| C (graphite) | 0.9            | 0.4            | 0.007   |
| Al           | 0.2            | 0.4            | 0.2     |
| Si           | 0.4            | 0.6            | 0.2     |
| Cu           | 0.3            | 1.1            | 0.4     |

#### *Grazing Incidence*

Calculations for grazing incidence mirrors include the effect of energy density dilution through the angle (the footprint area increases), reflectivity, and deposition throughout an e-

folding depth for the photons. The results demonstrate an interplay between atomic number, incidence angle, and photon energy. The absorbed energy density is [4]:

$$\eta_A (eV / atom) = E_{Pulse} \left( \frac{\theta_i}{D_w^2} \right) \left( \frac{1-R}{\delta_p \rho} \right) \quad (5.1)$$

Here  $E_{Pulse}$  is the energy of the FEL pulse in eV,  $D_w$  is the beam diameter at the optic,  $\delta_p$  is the 1/e penetration depth of the light into the material in a direction normal to the surface,  $\rho$  is the atomic density of the material, and R is the reflection coefficient. Following conventional analysis [2,4], we show  $\eta_A$  vs.  $\theta_i$  in **Figure 9.1** for three candidate reflecting materials: Au (high-Z), Ni (medium-Z), and Be (low-Z) located at the front of Hall A. Three representative energies characteristic of the LCLS's coherent fundamental and 3rd harmonic are shown (900 eV, 8600 eV, and 30000 eV). Selecting  $\eta_A \leq 0.01$  (a criterion suggested by earlier experimental work at SSRL [5] and safe with respect to melt), and an incidence angle of 0.5 mrad, we may safely use a Ni- or Au-coated mirror for low energies (1 keV) and very high energies (30 keV), and a Be-coated mirror for intermediate energies (8 keV).

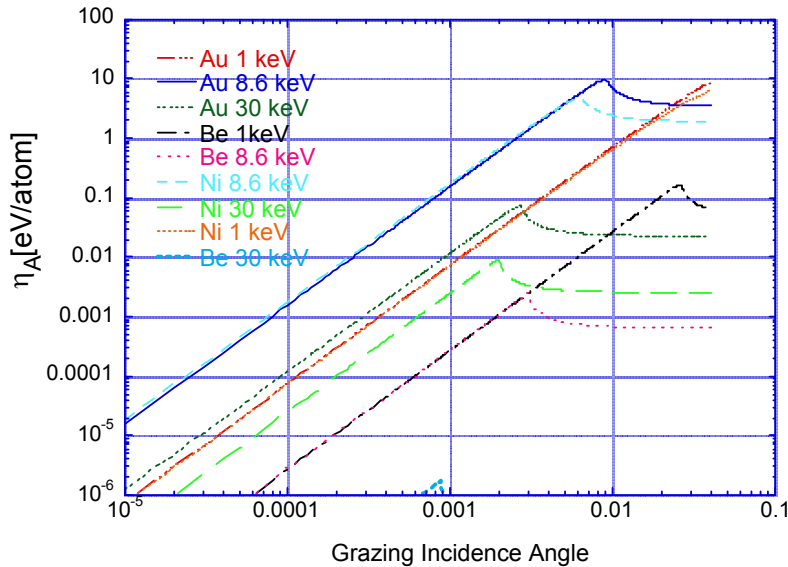


**Figure 9.1** Peak power energy loading of candidate LCLS mirror materials vs. (TE) grazing incidence angle and LCLS energy.

*Diffraction*

The reflection bandwidth of a perfect crystal is much smaller than the bandwidth of the FEL beam. This means that nearly all of the FEL beam will not be diffracted but will pass into the crystal, and therefore in estimating high-power effects one can neglect the diffraction process entirely and treat the reflecting crystal as a pure absorber. Unless grazing incidence geometry is

used, the angle of incidence on the crystal will not have a large effect on the power density, and so the calculations for normal incidence shown in **Table 9.2** can be used to estimate the probability of damage to the diffracting crystal. These calculations show that Be and diamond crystals should be safe to use as monochromators in Hall A. Si might also be considered at the high-energy end of the LCLS range.

**Table 9.3** summarizes the possible materials that can be used if there is no FEL radiation attenuation. In Hall B the increased spot size reduces the energy density by a factor  $\sim 15$ , and more standard materials are usable at all photon energies.

**Table 9.3** Summary of suitable materials for optical components, without any FEL radiation attenuation

|                     | Hall A                          |                             | Hall B   |          |
|---------------------|---------------------------------|-----------------------------|----------|----------|
|                     | 0.8 keV                         | 8 keV                       | 0.8 keV  | 8 keV    |
| Transmission        | Li, Be,<br>possibly B, C        | Li, Be, B, C<br>possibly Si | Anything | Anything |
| Grazing incidence   | Anything (extremely<br>grazing) | Be                          | Anything | Anything |
| Crystal diffraction | No good crystal<br>candidates   | Be, B, C<br>possibly Si     | Anything | Anything |
| Multilayers         | All low to moderate<br>Z        | All low to moderate<br>Z    | Anything | Anything |

Continued R&D into x-ray photon-material interactions and damage is imperative to test the calculations shown above. Not all known physics has yet been included in the modeling described above. More importantly, the remarkable photon densities are expected to instigate new processes, which are the specific topic of proposed atomic physics experiments. The effects of the intensity spikes within a single FEL pulse, with characteristic spike width less than 1 fs and intensity up to 5 times the nominal value, are unknown.

#### *Absorbers and Attenuators*

Gas, liquid or metal attenuators (see **Section 9.2.2.1**) will be constructed to reduce the FEL beam intensity, both as an experimental control, and to avoid damage to optical components and diagnostics. The gas attenuator [6] can be used for initial studies of scattering of the LCLS pulses by absorbing media, to answer some of the physics questions mentioned above. The chamber design includes ports for line-of-sight fluorescence detection, as well for the introduction of external magnetic and electric fields. Due to its location inside the Front End Enclosure, provisions for a detector shielding enclosure have been included.

## 9.2 Layout and Optics

### 9.2.1 Experimental Halls

Two experimental halls are planned, one close to the undulator exit (Hall A, starting about 50 m from the undulator end) and one considerably farther downstream (Hall B, starting about 400 m from the undulator end) (see **Figure 9.2**). The total experimental floor area will allow the installation of several experimental stations; the hall locations are determined by local access roads and topography. Optics in Hall B will experience a reduced power density that should allow a wide range of materials to be used for samples and optical elements. Hall A will be useful for those experiments requiring maximum power density.

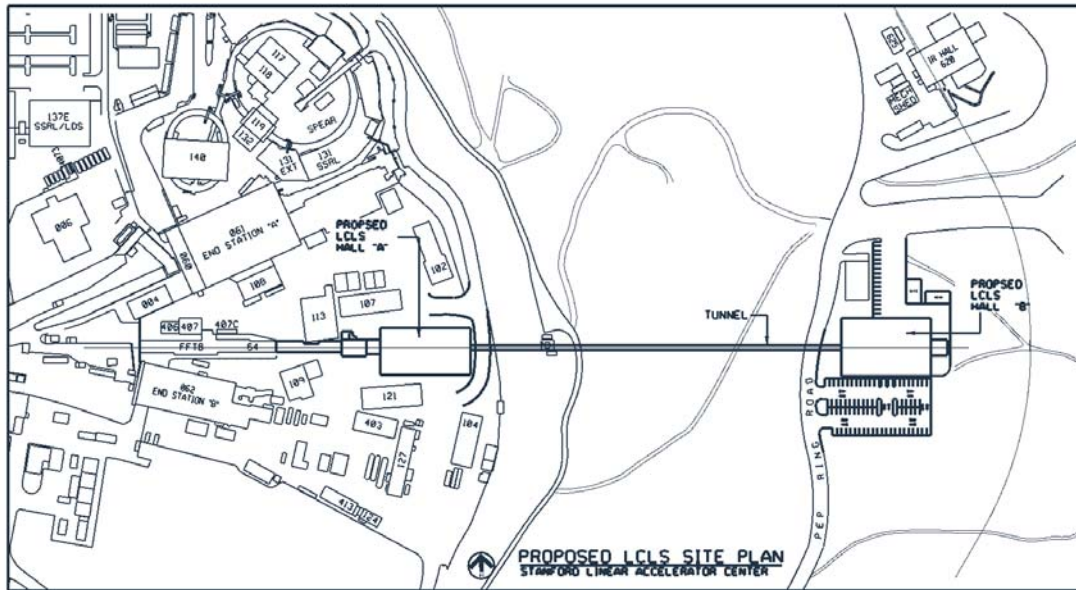


**Figure 9.2** LCLS site plan showing experimental halls.

An additional reason for a near hall (Hall A) involves the transmission of the spontaneous synchrotron radiation (SR) to experiments. Close to the undulator, a few-mm aperture should transmit a usable fraction of this spectrum. Transporting the same SR cone to the far hall would require an unworkably large vacuum aperture.

The large flight distance to Hall B will place some stringent requirements on beam pointing accuracy (the specification of beam wander in the LCLS design study report is  $\sim 10\%$  of the beam diameter, independent of path length). However, similar stringent stability requirements must implicitly be met for reliable SASE FEL operation — the angular acceptance for SASE saturation through the undulator is on the same order as the beam divergence, so any beam angle excursions

larger than this value would probably quench any coherent output (a similar constraint applies to the position of the beam axis). To achieve this level of accuracy, it may be necessary to stabilize the system against slow drifts with an active monitor and feedback system.

The remainder of **Section 9.2** describes the optical layout and optical elements in detail.

## 9.2.2 Optical Enclosures

### 9.2.2.1 Front End Enclosure

Elements in the Front End Enclosure (see **Figure 9.3**) include fixed masks, a fast valve, vertical and horizontal slits (2 of each), a gas attenuator, a variable-thickness solid attenuator, and a beam stop including a burn-through monitor.

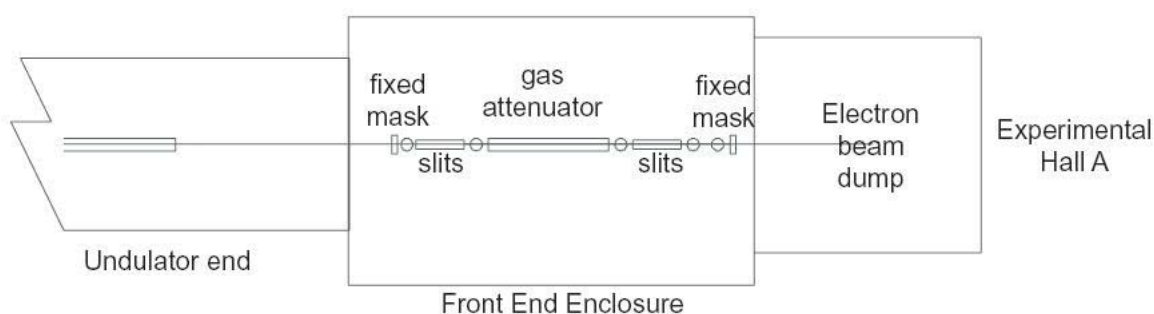


**Figure 9.3** Layout of the Front End Enclosure

#### *Fixed Mask*

The very first element of the photon transport system is a fixed mask, located 9 m downstream from the undulator, where it will not be hit by the deflected electron beam. The purpose of this mask, and a similar one located at 28 m from the undulator, is to insure that all radiation allowed downstream is confined within a very small angular region. This in turn will insure that all radiation in the first experimental hall stays within the beam pipe. Separated by 19 m and each having an aperture with diameter 4.5 mm, the fixed masks limit the transmitted angular range to 240  $\mu\text{rad}$  (FWHM). At the back end of Hall A, this transmitted angular range would have a diameter of 16 mm, well-contained within the beam pipe.

The aperture diameter of the fixed masks, 4.5 mm, is much larger than the diameter of the coherent FEL beam (note that the masks are nearly as large as the beam pipe through the undulator). Within the rather limited mis-steering range that will support FEL amplification, there is no possibility that the coherent radiation will strike the fixed masks. Thus, their purpose is only to intercept the wings of the spontaneous radiation. The peak-power densities at the masks will not be problematic, and they can be made from standard metal x-ray absorbers. Average power levels on these masks will be negligible, though water-cooling will be included.

### *Fast Valve*

Provision is made for a fast ( $< 0.1$ sec) vacuum valve, to protect the upstream vacuum system in the event of vacuum failure in the experimental area. The sensors that trigger this valve will be interlocked with the linac controls, so that the valve will not be subjected to FEL radiation.

### *Vertical Slit and Horizontal Slit*

The x-ray beam entering the x-ray optics system consists of an intense coherent FEL line with an FWHM angular divergence of about  $1 \mu\text{rad}$  ( $9 \mu\text{rad}$ ) for an electron energy of 15 GeV (5 GeV), surrounded by a broad spontaneous distribution with an FWHM angular width of about  $250 \mu\text{rad}$  ( $780 \mu\text{rad}$ ). For particular experimental applications, the spontaneous radiation can constitute a noise source and will need to be removed. These considerations have led to the introduction of the two-slit-pair system shown in **Figure 9.4**. Each slit assembly consists of a two movable jaws defining an adjustable horizontal aperture, and two movable jaws defining an adjustable vertical aperture. The first slit assembly is located just upstream of the absorption cell so that low energy spontaneous radiation can be filtered out for scattering experiments located at the cell. The second slit-pair, located about 15 m farther downstream, can also be used as an independent aperture, or combined with the first slit-pair to provide an angular collimator with an extremely small acceptance, providing a broad range of spectral-angular filtering options, including the delivery of quasi-monochromatic beams. An additional function of the slits (when operated in a collimator mode) will be to protect downstream optics such as mirrors from excessive peak power damage due to beam jitter.

Because the slit assemblies are located close to the FEL source, the peak power density needs to be considered. It is not intended for the slits to actually intercept the FEL beam, but in order to effectively cut out the spontaneous radiation background the slit jaws must come very close to the FEL beam. Two slightly different concepts for the slit jaws are under consideration. One concept treats the slit jaw as a grazing-incidence mirror, reflecting unwanted radiation out of the main beam path, and into a downstream mask. This slit jaw would be best coated with a highly-polished layer of high-Z material. At grazing incidence, this material could survive the spontaneous radiation and the wings of the FEL radiation. The other concept treats the slit jaw as a pure absorber at normal incidence. If made of Be it could withstand the spontaneous radiation and the wings of the FEL radiation. Further analysis of the expected radiation pattern will help determine which concept is better.

Either concept requires a long slit jaw with precision motion control. We propose to use a modified version of an existing SLC collimator design as presently employed in the SLAC beam switchyard for collimator C-0 and momentum slit SL-2 [7], with new jaws. The jaws will be water-cooled for optimal dimensional stability during operation. The jaws are remotely adjustable by means of stepper motors and can be differentially adjusted to control  $d_{UV}$ ,  $d_{dV}$ ,  $d_{UH}$ , and  $d_{dH}$  (see **Fig. 9.4**), as well as the average vertical and horizontal midplanes of the slits. A maximal incidence-angle range of about 0-1.5 mrad is envisaged and the minimum aperture size will be variable from 0 to  $>1$ cm.

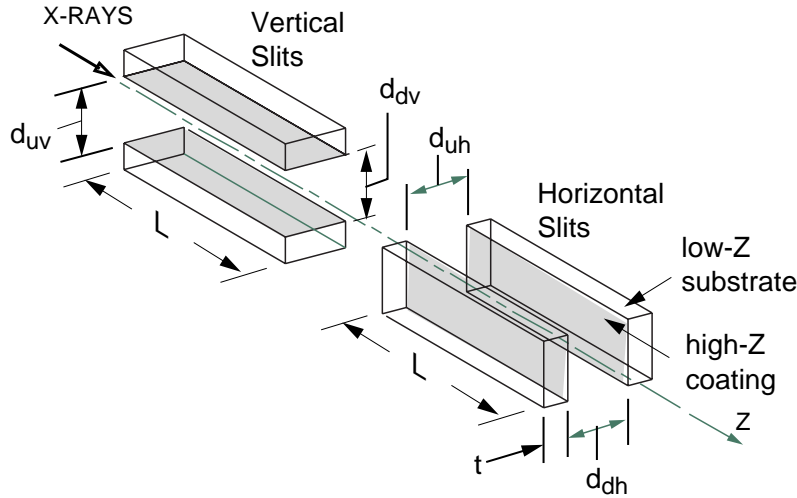


**Figure 9.4** The LCLS x-ray slit configuration. Gap dimensions  $d_{uv}$ ,  $d_{dv}$ ,  $d_{uh}$ ,  $d_{dh}$  are independently adjustable.

The total footprint of the spontaneous radiation at both slit locations will be significantly larger than the upstream slit apertures  $d_{uv}$  and  $d_{uh}$ . This means that not only can one or more of the slits absorb most of the spontaneous x-ray power during operation, but also that most of it will impact the jaws' upstream facets at normal or near-normal incidence. At the locations of the slits, the spontaneous peak power density at normal incidence can attain off-axis values that are only three orders of magnitude below that of the coherent line, which brings the peak power densities anticipated for the jaws to levels at which little or no experimental data exists. Similar peak power levels in the high-Z reflecting material (assuming ~99% reflectivity) can be expected for scenarios where the LCLS coherent line impacts the jaw surface, due to jitter or for other reasons.

Although there is some evidence of survival of mirrors exposed to very high specific power densities from alternative sources, the processes that take place in the temporal and spectral regimes of the LCLS [8] are still very poorly understood and more experimental and theoretical studies will be needed.

#### *Attenuator/Absorber*

Controlled attenuation of the coherent pulses of the LCLS could be accomplished by passage through a gas, solid, or liquid. Over the long-wavelength range of the LCLS fundamental (800 eV to about 4 keV), it is unlikely that any solid absorber (except perhaps one made of pure lithium) would survive undamaged in the Front End Enclosure (see **Figure 9.5**). For shorter wavelengths, absorption cross sections are lower, and a solid absorber made of light elements is practical.

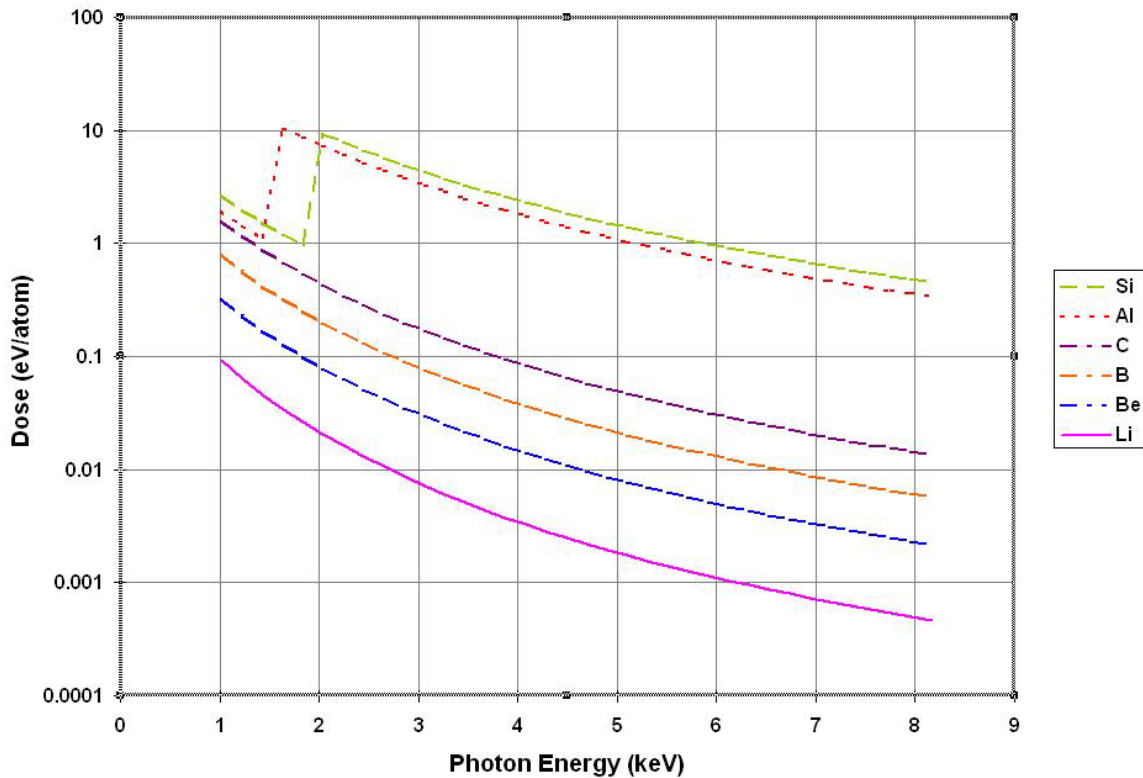


**Figure 9.5** Energy dose absorbed from one shot of LCLS for different absorber materials, at a location in the Front End Enclosure.

Therefore, in addition to conventional solid absorbers, LCLS plans to use a gas absorber cell, using high-pressure puff valves to introduce the absorbing gas into the path of the coherent FEL photons (see **Figure 9.6**) [5]. The axial dimensions of the chamber and the number of valve nozzles must be adequate to allow a sufficient thickness of the gas to provide two or more orders of magnitude of attenuation over the 800-4000 eV range. The combined axial and transverse dimensions are determined by the requirement of maintaining an average vessel pressure of  $<0.0075$  Torr, corresponding to the Knudsen-through-molecular flow regimes [9]. This pressure, which is sufficiently low to be reduced to  $<10^{-6}$  Torr by the differential pumping sections bracketing the chamber, will be determined primarily by:

- 1) the average volume of gas introduced into the chamber per puff;
- 2) its average pressure;
- 3) the axial conductance out of the gas cell;
- 4) the chamber volume;
- 5) the puff valve repetition rate; and
- 6) the capacity of the primary pump(s) connected directly to the chamber.

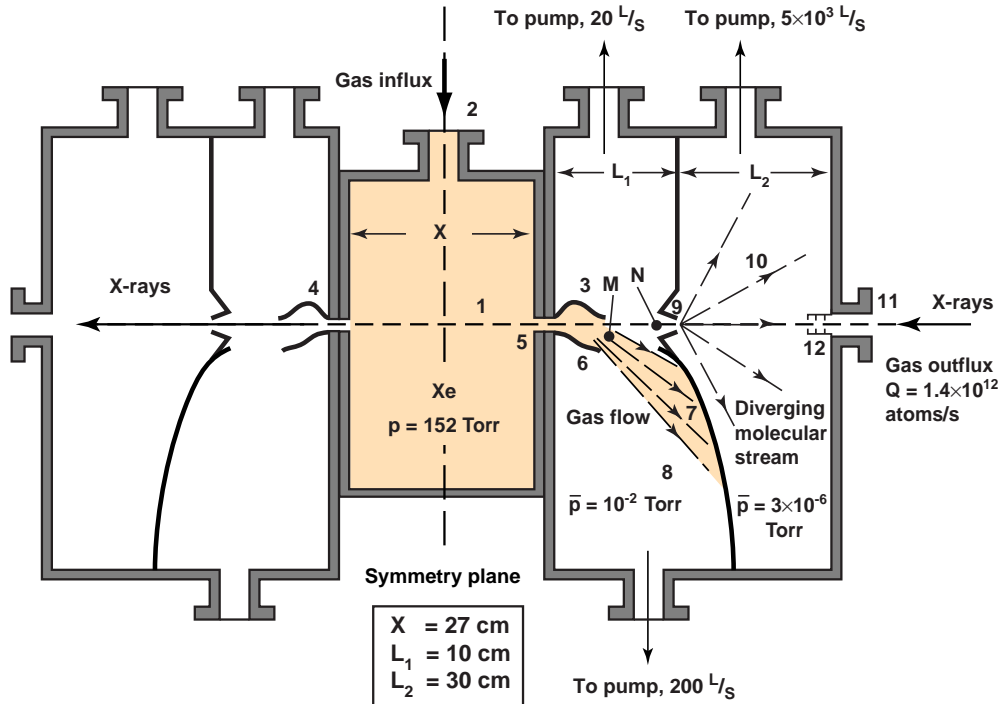


**Figure 9.6** The conceptual design for the gas cell attenuator

The operation of the gas cell in the weak-field (linear) regime using xenon as an absorber has been calculated for reference. In **Figure 9.7** the absolute attenuation of x-rays through xenon for four given pressure,  $t_g$ , [Torr-cm] products is plotted from 800 to 25000 eV. The curves indicate that a 2000 Torr Xe gas jet with  $t_g=1$  cm would provide at least two orders of magnitude of attenuation over the low-energy range of LCLS (800–4000 eV). Note that this absorption calculation assumes that the absorption mechanisms are essentially uni-molecular and linear. With suitable design and a sufficiently low repetition (pulse) rate the loading of the vacuum system by the required amount of gas should be maintainable at acceptable levels.

Weak-Field Attenuation Curves for Xenon vs. (Pressure x Distance)

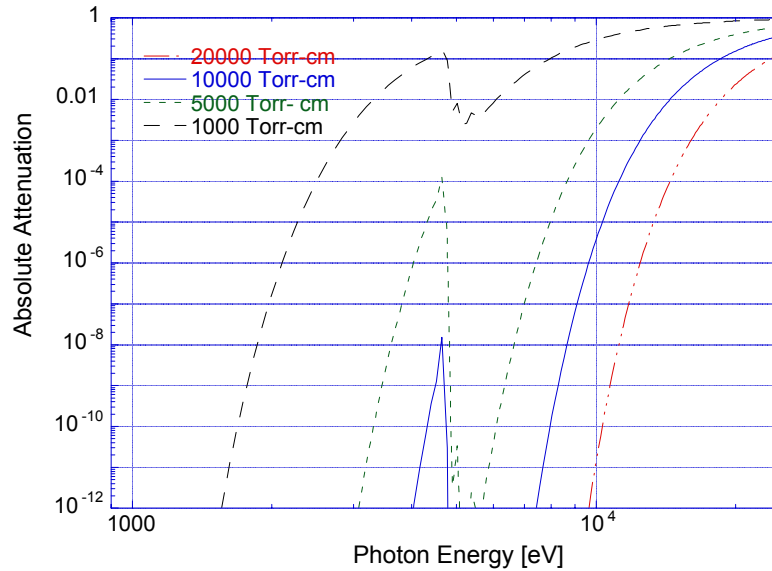


**Figure 9.7** Weak-field attenuation curves for xenon.

The absorption cell can also be used for initial studies of scattering of the LCLS pulses by absorbing media. The chamber design includes ports for line of sight fluorescence detection, as well for the introduction of external magnetic and electric fields. Due to its location inside the FFTB tunnel, provisions for a detector shielding enclosure have been included.

While the absorption of xenon in the linear regime can be calculated, some corrections may be required for the actual LCLS pulses, whose intensity and degeneracy parameters lie well outside the regime of weak-field interactions. Fundamental questions remain about the effects of nonlinear scattering and absorption processes on the temporal shape and the longitudinal and transverse coherence of the pulses.

#### *Solid Attenuator*

At energies above 4 keV, solid attenuators become practical. **Figure 9.5** above shows that the absorbed dose in B and C has a reasonably safe value of less than 0.1 eV/atom for FEL energies above 4 keV. This suggests that B<sub>4</sub>C would make a good absorber material. **Table 9.4** shows the B<sub>4</sub>C thicknesses needed to vary the attenuation linearly from 0.1 to 1 and logarithmically from 10<sup>-1</sup> to 10<sup>-10</sup>, for an x-ray energy of 8 keV.

**Table 9.4** Thicknesses of boron carbide required for attenuation of 8 keV x-rays

| Linear attenuator   |                                 | Logarithmic attenuator |                                 |
|---------------------|---------------------------------|------------------------|---------------------------------|
| Desired attenuation | B <sub>4</sub> C thickness (mm) | Desired attenuation    | B <sub>4</sub> C thickness (mm) |
| 1                   | 0                               | 10 <sup>-1</sup>       | 4.1                             |
| 0.9                 | 0.2                             | 10 <sup>-2</sup>       | 8.1                             |
| 0.8                 | 0.4                             | 10 <sup>-3</sup>       | 12.2                            |
| 0.7                 | 0.6                             | 10 <sup>-4</sup>       | 16.3                            |
| 0.6                 | 0.9                             | 10 <sup>-5</sup>       | 20.4                            |
| 0.5                 | 1.2                             | 10 <sup>-6</sup>       | 24.4                            |
| 0.4                 | 1.6                             | 10 <sup>-7</sup>       | 28.5                            |
| 0.3                 | 2.1                             | 10 <sup>-8</sup>       | 32.6                            |
| 0.2                 | 2.8                             | 10 <sup>-9</sup>       | 36.7                            |
| 0.1                 | 4.1                             | 10 <sup>-10</sup>      | 40.7                            |

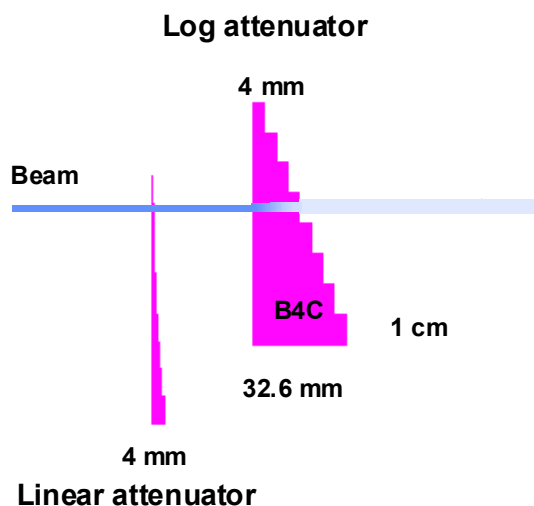


**Figure 9.8** A linear/log attenuator system

The attenuators will be fashioned from single plates of B<sub>4</sub>C milled in a staircase pattern to the thicknesses specified in **Table 9.4** as shown in **Figure 9.8**. The linear and logarithmic attenuators will be mounted on separate translation stages allowing all combinations of linear and logarithmic attenuation to be applied.

The attenuator translation stages will provide motion in the X and Y directions with a precision of  $< 1$  mm.

#### *Diagnostics Tanks*

Space is available downstream from the gas and solid attenuators for beam diagnostic measurements such as pulse intensity and pulse shape. The diagnostics will monitor the operation of the attenuators. See **Section 9.4.2**.

#### *Beam Stop with Burn-Through Detector*

At the downstream end of the Front End Enclosure there is an insertable beam stop. This device consists of an upstream beryllium section to reduce the peak power of the FEL beam, and downstream copper and heavy metal sections to absorb the full spectrum of the LCLS. The beam stop includes an integral burn-through detector, which, in case the beryllium section fails to insert, will protect the radiation absorbers and shut down the LCLS. The radiation absorbers are duplicated with separate control systems so that the risk of a radiation accident is negligible.



**Figure 9.9**      Concept of the insertable beam stop with burn-through detector.

#### **9.2.2.2 Hutch A1**

The first hutch in Hall A (**Figure 9.10**) will contain optical elements which condition the x-ray beam for the Hall A experiments. Only one such element will be included in the initial LCLS, though space is made available for future optics. Hall A is intended primarily for high-intensity experiments, using the full bandwidth of the coherent FEL beam.

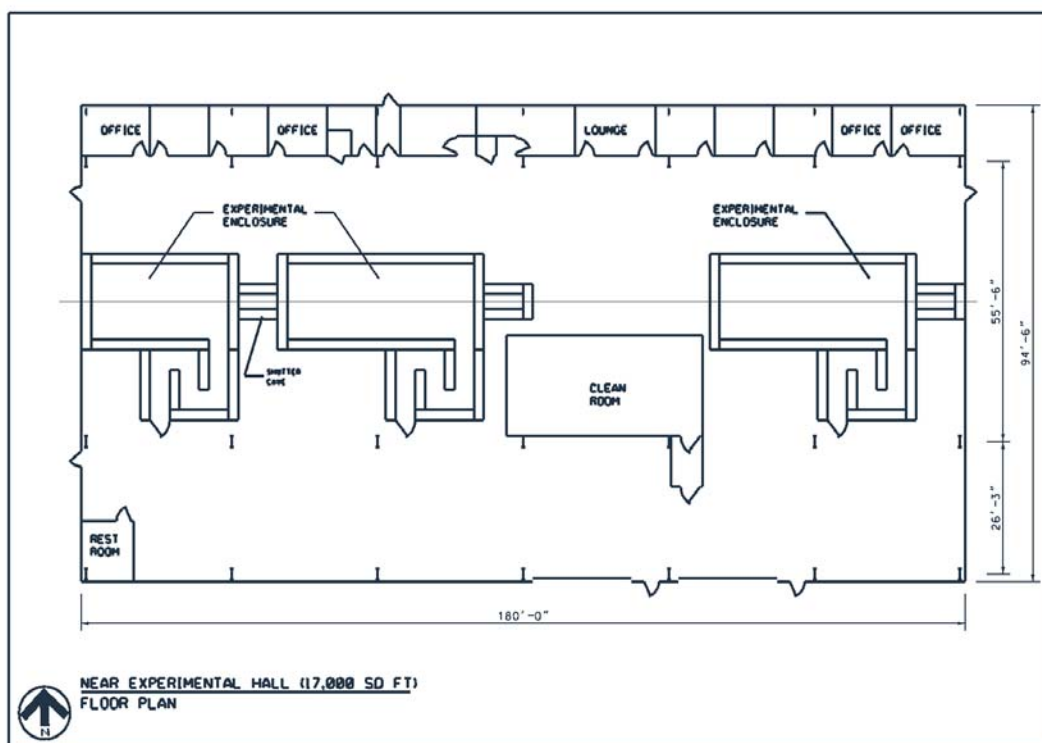


Figure 9.10 Layout of Experimental Hall A

### *Dual-Mirror Harmonic Rejection System*

Some experiments (in particular, atomic physics experiments) need a very clean spectrum without higher harmonics. With a small aperture upstream, the LCLS spectrum contains only odd harmonics. The strongest higher harmonic, the third, is expected to experience some FEL amplification, but its intensity will be about two orders of magnitude below that of the fundamental. A pair of grazing-incidence mirrors can add several more orders of magnitude to that ratio.

The separation of the 3<sup>rd</sup> harmonic contaminant requires a grazing incidence mirror system with graze angle above the critical angle for the 3<sup>rd</sup> harmonic while lower than the critical angle for the fundamental component. It is possible to trade total reflectance of the primary radiation for suppression of the 3<sup>rd</sup> harmonic. By increasing the angle of incidence closer to the critical angle for the fundamental, greater suppression of the 3<sup>rd</sup> harmonic is possible; but at the price of reduced reflectivity in the fundamental. Reflectivity of the 3<sup>rd</sup> harmonic will be on order a few percent. Because of this modest rejection capability, and to simplify the beamline geometry, a two-mirror system is the appropriate choice.

The harmonic separator mirrors are parallel to one another; and the second mirror has angle adjustment available to fine-tune the direction of the outgoing beam. The slope error in the mirrors must be kept below a fraction of the natural beam divergence and leads to severe, though technically achievable, figure constraints. The opto-mechanical tolerances are given in **Table 9.5**.

**Table 9.5** Mirror requirements

| Parameter           | Requirement  | Specification   |
|---------------------|--|---|
| Slope Error         | Negligible contribution to beam divergence.  | Better than 0.5 $\mu$ rad slope error, or 5nm over typical 10mm ripple wavelength.<br><br>Flatness to 1/200 wave RMS, 1/40 wave P-V   |
| Surface roughness   | Scattering losses below 10%  | Surface finish < 20 nm RMS.   |
| Size                | Intercept beam over angular range of 0.7 to 1.5 degrees                                      | 50 mm total length.   |
| Angular positioning | Allow tradeoff between 3 <sup>rd</sup> harmonic suppression and fundamental efficiency       | Mirrors free to rotate from 0 to 2 degrees both slaved and independently. Rotation error throughout this range must be < 1 $\mu$ rad. |
| Lateral positioning | Illuminate repeatable areas on mirrors. Ability to operate beamline without order separator. | Translate mirrors completely out of beam and reposition them to better than 10 $\mu$ m tolerance.                                     |

The flatness constraint will be met by means of iterative polishing. Grain structure in Be is considered to be a near insurmountable barrier to achieving both the surface finish and the final figure requirement. Meeting these requirements in Si is, though non-trivial, well within the capability of existing commercial vendors. A hybrid optic material, e.g., sputtered Be on a Si substrate, is a possibility although the thermal loads on the Si are negligible. A detailed thermal study will be needed to confirm initial calculations that the several degree rise in temperature on the mirror surface expected during operation will not increase figure error. The mismatch between the coefficient of thermal expansion for Be and Si (Be is 3 times higher) may effectively bar the use of a (non-cooled) hybrid material.

Flatness must be maintained once the mirrors are mounted without inducing any stress into the optic. Angular motion that meets these specifications will be achieved with a Picomotor driven flexure using an approach proven successful in the LLNL EUVL effort [10].

#### *Spools, Chambers, and Beam Stop*

Hutch A1 contains a diagnostics chamber for diagnostics associated with adjustment of the mirrors. It also contains several spool pieces, which may in future be replaced by additional mirror systems and monochromators. At the back end of Hutch A1 is an insertable beam stop with integral burn-through detector.

#### **9.2.2.3 Hutch A2**

Hutch A2 will house LCLS experiments. It will also contain beam-conditioning optics, which need to be close to the experiments, in particular, focusing systems with short focal length.

### Kirkpatrick-Baez Focusing System

One effective technique for focusing x-rays to sub-micron spot diameter uses total external reflection mirrors in the Kirkpatrick-Baez, (KB), geometry (see **Figure 9.11**). To achieve small spot size the KB mirrors must exactly hold a precise elliptical geometry. Using bending fixtures to apply a precise bending moment to each end of a mirror, a near perfect figure can be obtained from a previously figured flat. Sub-micron spot size has been demonstrated from a system of this type [11] and ray tracing results indicate that beams with cross sections of less than  $0.04 \mu\text{m}^2$  (gains in excess of  $10^5$ ) are achievable.

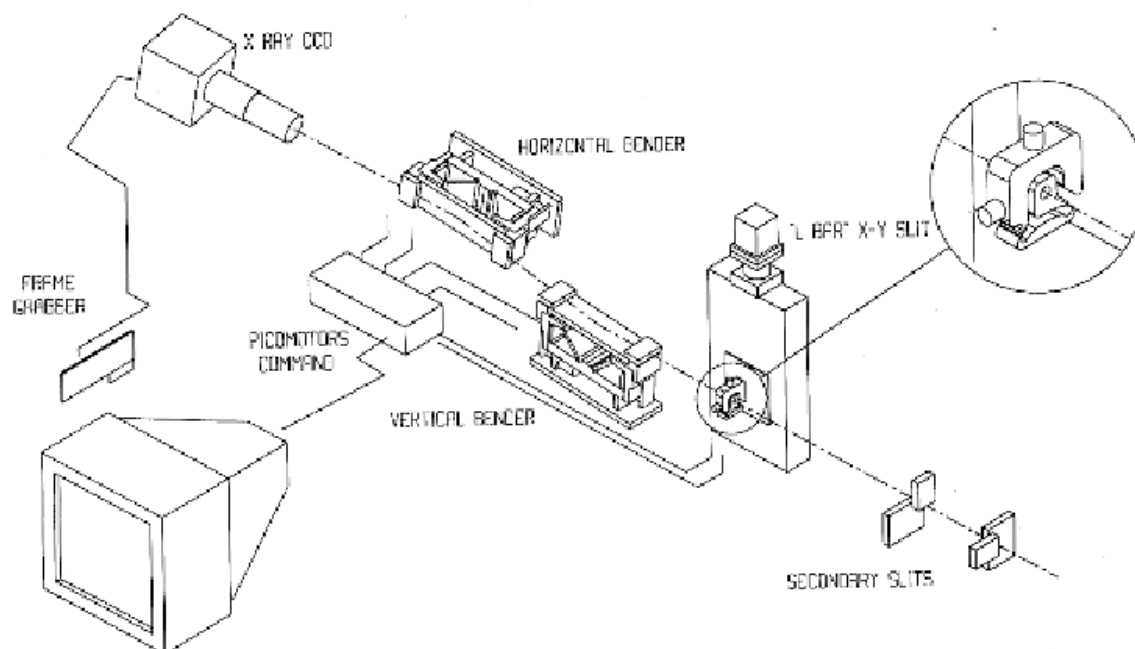


**Figure 9.11** Schematic of the Kirkpatrick-Baez system

Improvement on current results requires improvement in the mirror figure; specifically it requires better conformance to the ideal elliptical profile. Our approach will be to simplify the typical bending arrangement by applying a bending moment to one end of the mirror. The mirror cross-sectional thickness will vary as a function of length along the mirror. Analytic optimization of the thickness profile allows us to accurately predict the deformation of the mirror under the applied bending moment and precisely control the resultant figure.

A significant advantage of the KB approach is that the mirror substrates must only meet the (exacting) specifications for the flat mirrors used for the order separator. Angular and bending moment adjustments for the mounts also have similar specifications. It has recently been demonstrated [10] that deposition of thin films on the surface of can be used to allow control of figure at the nm level.

### Refractive Focusing System

Another promising system for focusing the FEL beam involves refractive optics. It is straight forward to show that low-Z refractive optics can withstand the full power loading of the 8 keV FEL and therefore can be used with confidence for applications desiring to achieve the highest power levels in the focal spot. A low-Z refractive focusing optic for the LCLS will consist of one or more “blazed phase plates”, which are the most general form of refractive optics. The lenses will be made by replicating diamond-turned forms in C and/or Li.

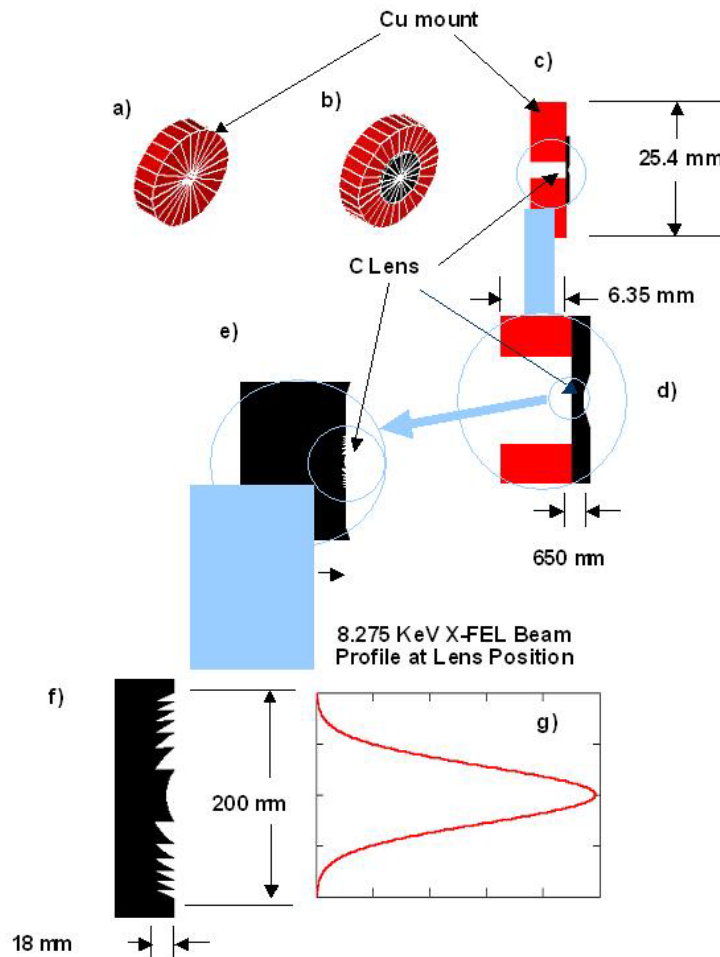


**Figure 9.12** Refractive focusing optics for LCLS

**Figure 9.12** shows details of a single lens design. The lens is carved into the face of a C (graphite) disk and mounted over a hole drilled through a 25.4 mm diameter Cu mount. The graphite disk is 650 microns thick except in the center where it thins down to 400 microns. The active portion of the lens is 200  $\mu\text{m}$  in diameter and consists of 6 concentric grooves machined to a maximum depth of 18.8  $\mu\text{m}$ . The plot of the LCLS beam profile at the lens, **Figure 9.12g**, shows that the 200- $\mu\text{m}$  lens diameter nicely captures most of the beam.

The shape of the grooves is determined by calculating, at the position of the lens, the phase change necessary to convert the diverging Gaussian FEL beam into a converging Gaussian

waveform whose waist is at the sample position. The radial phase profile was converted to a depth profile by multiplying by the optical constant for graphite, which is  $18.8 \mu\text{m}/2\pi$  radians phase change (with respect to vacuum) at 8.275 keV.

Several of these lenses will be stacked into single machined mount to achieve shorter focal lengths.

### Apertures

Apertures must be used to eliminate the halo of stray radiation surrounding the focal spot. Survivability is an issue in the design of the apertures in Hutch A2. The basic concept is to utilize a laminate consisting of 4 mm of  $\text{B}_4\text{C}$ , 150 microns of Al, and 200 microns of Ta. This laminate has sufficient absorption to block x-rays up to the 3rd harmonic. Furthermore the  $\text{B}_4\text{C}$  attenuates the direct FEL beam enough to prevent damage to the Al, which further attenuates the beam enough to prevent damage to the Ta.

A series of holes having diameters from 1 mm down to 100 microns will be drilled through the laminate, which will then be mounted on a movable stage that provides both rotation and translation of the laminate. A second, fixed, laminate having a single 1 mm diameter hole keeps light from passing through all but a single hole in the movable laminate (**Figure 9.13**). The ability to rotate the laminate is necessary because of the large aspect ratio of the holes. Using a downstream intensity monitor, and starting with the largest diameter hole, the movable laminate will be rotated into a position that maximizes the signal. The laminate will be shifted to the next smaller diameter hole and rotated again to achieve highest intensity downstream. This process will be repeated with successively smaller holes until the hole of the desired diameter is positioned and aligned.

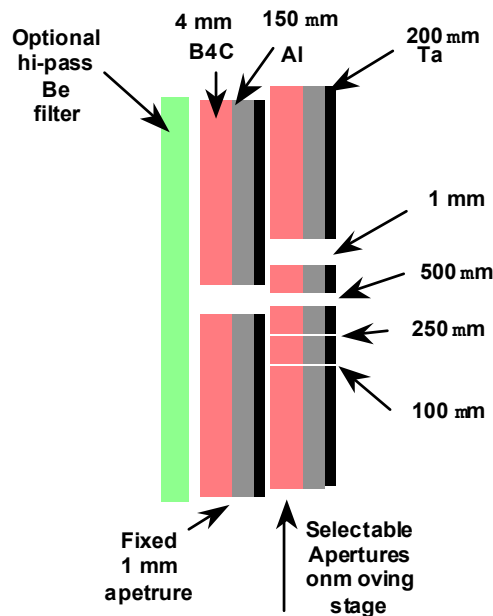


**Figure 9.13** Apertures for the FEL x-ray beam

The stages used to position the apertures will have positioning precision  $< 10 \mu\text{m}$  and angular precision of  $< 1 \text{ mrad}$ .

#### *Attenuator*

Some experiments require a local attenuator for calibration and to prevent damage to sensitive components during alignment. The local attenuator will have a design very similar to the solid attenuator located upstream in the Front End Enclosure (see **Section 9.2.2.1**).

#### *Beam Intensity Monitors*

Beam intensity monitors are required to measure the absolute flux incident on the samples and the amount of flux transmitted through the samples. These monitors will be of the ion chamber type described in the facility diagnostics section (**Section 9.4.2.3**).

#### *Sample Chamber*

The sample chamber in Hutch A2 will be instrumented for studies required to characterize the interaction between the FEL pulse and matter. In addition to sample holders and photon spectrometers, it will include electron and ion time-of-flight spectrometers.

#### *Beam Stop*

At the back end of Hutch A2 is an insertable beam stop with integral burn-through detector.

### **9.2.2.4 Hutch A4**

Hutch A4 will initially be used for commissioning diagnostics, which will be housed in a diagnostics tank. See **Section 9.4.2**.

#### *Fixed Mask and Beam Stop*

At the back end of Hutch A4 is an insertable beam stop with integral burn-through detector. Behind the beam stop is a fixed mask with 4.5 mm diameter aperture, identical to the fixed masks in the Front End Enclosure. As with those masks, its purpose is to cut the divergence of the spontaneous radiation, so that all transmitted radiation remains within the beam pipe. The coherent FEL radiation cannot strike this mask, and so peak power is not a concern.

### **9.2.2.5 Inter-Hall Transport**

A beam pipe connects the two main halls through a tunnel. It is about 250 m long. Access will be available along the length of the tunnel. In the center of the tunnel, a diagnostics tank will permit beam intensity and position measurements.

### **9.2.2.6 Hutch B1**

The first hutch in Hall B will contain optical elements, which condition the x-ray beam for the Hall B experiments (see **Figure 9.14**). Only one such element will be included in the initial LCLS, though space is made available for future optics. Hall B is intended primarily for experiments, which prefer to be far from the source, in order to reduce the peak intensity or to allow focusing to a minimum spot size.

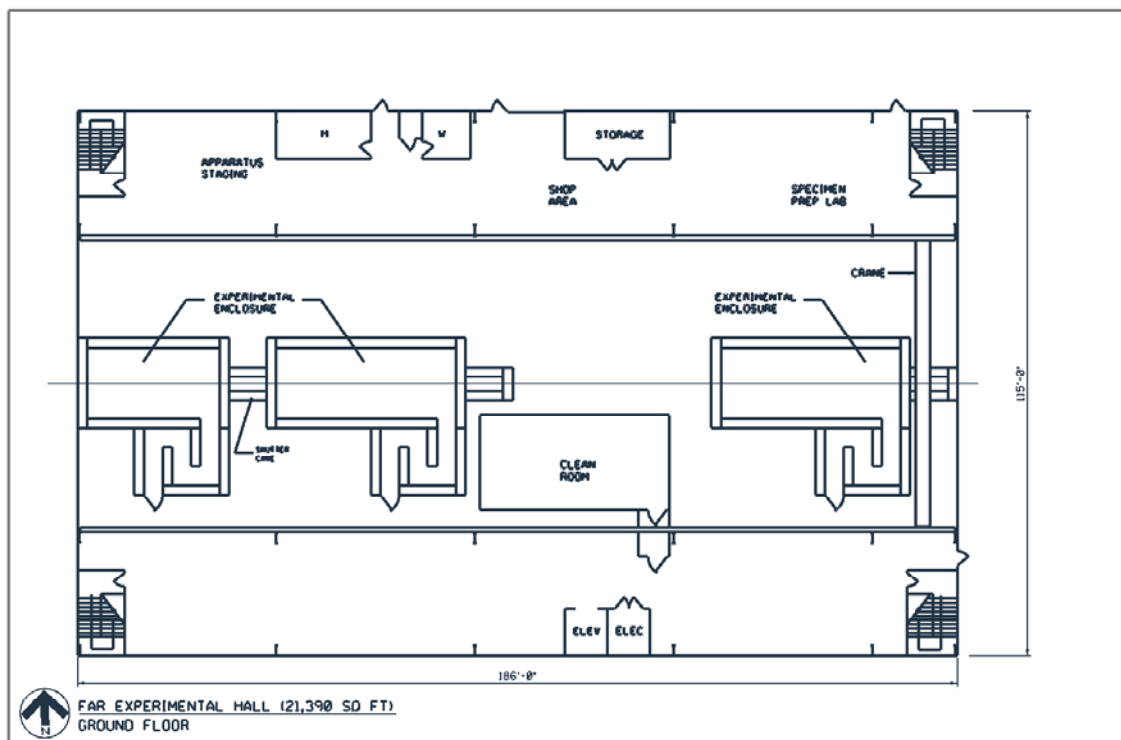


Figure 9.14 Experimental Hall B

### *Monochromator*

Some Hall B experiments will require a bandwidth narrower than the intrinsic bandwidth of the FEL. In Hall B, standard monochromator crystals such as silicon or diamond should not suffer any damage due to the peak power, and so standard crystal monochromator designs can be used [12].

### *Spools, Chambers, and Beam Stop*

Hutch B1 contains a diagnostics chamber for diagnostics associated with adjustment of the monochromator. It also contains several spool pieces, which may in future be replaced by additional mirror systems and monochromators. At the back end of Hutch B1 is an insertable beam stop with integral burn-through detector.

#### **9.2.2.7 Hutch B2**

Hutch B2 will house LCLS experiments. It will also contain beam-conditioning optics, which need to be close to the experiments, in particular, focusing systems with short focal length. Hutch B2 will also contain an optics tank with an x-ray pulse splitter and delay system, producing from each FEL pulse a pair of x-ray pulses with adjustable sub-ns delay.

### *Pulse Split/Delay*

This system will use crystal diffraction to split the FEL pulse, direct the two x-ray pulses around unequal path lengths, and bring them back onto the primary beam path with a time delay between them. **Figure 9.15** shows the proposed scheme. The beam-splitting is accomplished by a very thin (10  $\mu\text{m}$ ) silicon crystal. The radiation within the bandwidth for Bragg diffraction from this crystal is reflected with high efficiency (80%), whereas the radiation outside the Bragg bandwidth is efficiently transmitted (75% at 8 keV). By orienting the crystals in the two beam paths to reflect slightly different x-ray energies, the pulse is effectively split and sent around two separate paths. A simple translation can then be used to change the relative path lengths, and thus the pulse delay. The overall efficiency of the system for each path is about 30% at 8 keV. The bandwidth ( $\delta E/E$ ) for each crystal reflection is about  $2.5 \times 10^{-5}$ , so two pulse energies can easily be selected from the LCLS bandwidth of about  $10^{-3}$ .

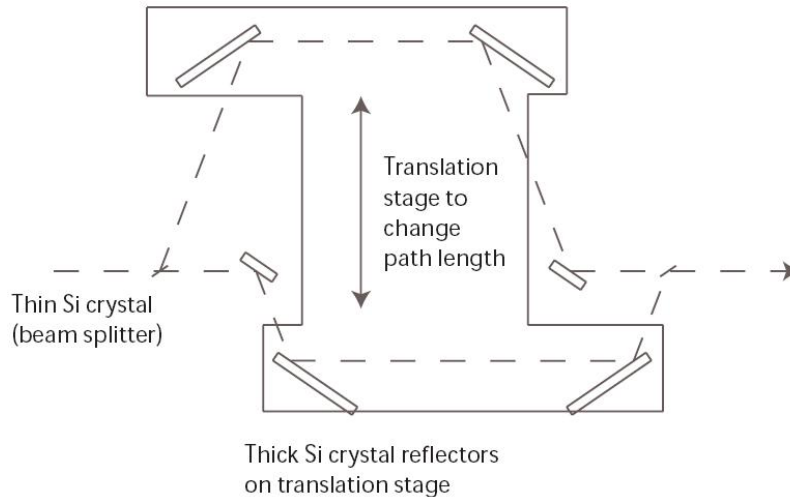


**Figure 9.15** Pulse split and delay technique. Delay values of several hundred picoseconds can be achieved, with accuracy of a few femtoseconds.

### *Focusing System*

Focusing in Hutch B2 will use a Kirkpatrick-Baez mirror system identical to that used in Hutch A2. If only one such mirror system is available initially, it can be transported and installed in either Hutch A2 or Hutch B2 as needed.

### *Apertures*

The apertures used in Hutch B2 will be very similar to those used in Hutch A2.

### *Attenuator*

Some experiments require a local attenuator for calibration and to prevent damage to sensitive components during alignment. The local attenuator will have a design very similar to the solid attenuator located in the Front End Enclosure.

### Beam Intensity Monitors

Beam intensity monitors are required to measure the absolute flux incident on the samples and the amount of flux transmitted through the samples. These monitors will be of the ion chamber type described in the facility diagnostics section (**Section 9.4.2.3**).

### Sample Chamber

The sample chamber in Hutch B2 will be instrumented for development of sub-picosecond time-resolved experiments, such as laser pump/x-ray probe and x-ray pump/x-ray probe experiments. It will include a goniometer for holding crystal samples, and windows for laser and scattered x-ray beams.

### Beam Stop

At the back end of Hutch B2 is an insertable beam stop with integral burn-through detector.

#### 9.2.2.8 Hutch B4

Hutch B4 may be used for future facility diagnostics.

### Beam Stop

At the back end of Hutch B4 is a fixed (not insertable) beam stop. Power levels at this point will not damage materials such as copper, and so no burn-through monitor is required.

## 9.3 Mechanical and Vacuum

The beam transport mechanical and vacuum system contains approximately 400 meters of vacuum beam pipe and is maintained at  $10^{-7}$  Torr by approximately 70 ion pumps. The basic design of a section of beam pipe is shown in **Figure 9.16**. These sections are repeated through the halls and tunnel, except in places where the pipe is replaced by one of the tanks or other instruments in the beam line.

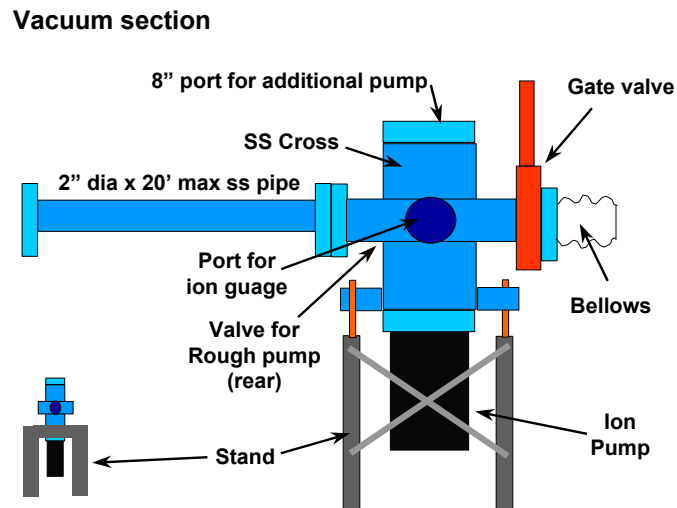


**Figure 9.16** Typical section of vacuum beam pipe

The pipes are 2" stainless steel electroplated inside and out and connected with metal sealed gaskets and welded 4 5/8" Conflat flanges. The maximum pipe length is 20 feet. The pumping section consists of a stainless-steel cross with 8" flanges top and bottom to accommodate the ion pumps. Each ion pump has its own power supply. Additional 4 5/8" ports on the beam left and right accommodate ion gauges and a valve for rough pumping. The section terminates with an isolation valve and a bellows for alignment. The isolation valves are all metal gate valves such as manufactured by VAT. The stands are plasma-cut plates with cross bracing for earthquake protection.

The isolation valves around some of the tanks contain integrated welded Be windows, in order to allow x-ray experiments to take place in rough vacuum or in air, if desired. The windows are Brush-Wellman pinhole-free S-65 polished Be disks 46 mm in diameter and 250 microns thick.

Some LCLS optics tanks (e.g., the mirror tanks) require ultra-high vacuum conditions. Other tanks (e.g., the gas attenuator) require pressures much higher than  $10^{-7}$  Torr. These special tanks will be isolated from the main vacuum system by differential pumping sections. There are commercial differential pumping systems, which can do this job [13].

## 9.4 Diagnostics

### 9.4.1 Diagnostics Layout

The diagnostics are located in "diagnostics tanks" distributed along the beam line as shown in **Figure 9.17**. The diagnostics fall into two categories: 1) facility/monitoring diagnostics, and 2) commissioning diagnostics.

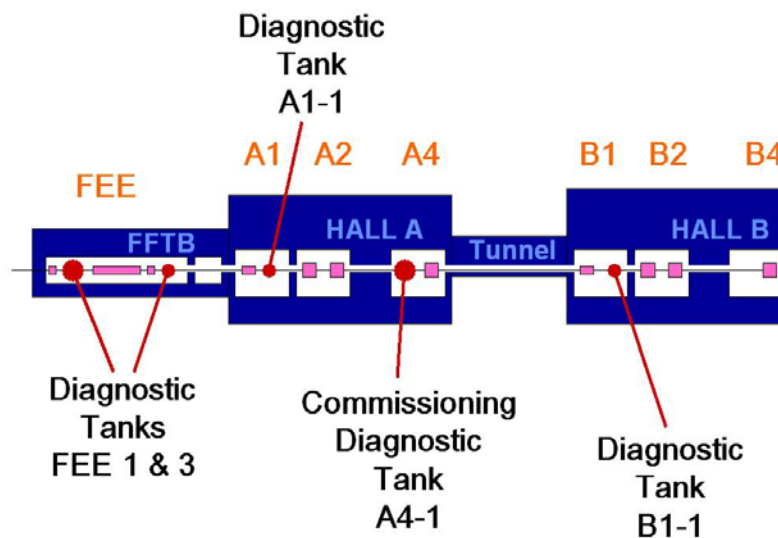


**Figure 9.17** Tank locations for LCLS x-ray diagnostics

The facility diagnostics mainly provide pulse-to-pulse information about the beam energy, spatial shape, and centroid, as it is transported through the beam transport system to the

experimental halls. Because of the fluctuating nature of the SASE FEL, it is critical to monitor these beam parameters on a pulse-by-pulse basis. This information is used to 1) provide feedback on the FEL performance, 2) aid in adjusting, monitoring, and setting facility optical systems (slits, attenuators, monochromator), and 3) provide energy, shape, and centroid information to users.

These diagnostics are located after the slits and attenuators in the Front End Enclosure, after the mirrors in the upstream end of Hall A, after the monochromator in the upstream end of Hall B, and at the very end of Hall B. They are intended to be "non-intrusive" if possible, allowing most of the beam to pass through without substantial modification. Avoiding some type of modification (coherence, intensity, etc.) may be difficult, especially at the lowest FEL photon energy.

The commissioning diagnostics are intended to measure the basic FEL performance parameters during commissioning and may be "intrusive". The goals of the commissioning diagnostics are to measure

1. Total pulse energy;
2. Pulse length;
3. Photon energy spectrum;
4. Transverse coherence;
5. Spatial shape and centroid location; and
6. Divergence.

The pulse energy, pulse length, spectrum and transverse coherence measurements will be performed in the "commissioning diagnostics tank" in Hutch A4. The divergence and shape measurements will be made by the "facility diagnostics" distributed along the beam line.

Characterizing the performance of LCLS will require pulse-by-pulse measurements of total energy, pulse length, spectrum, divergence, spatial shape, and transverse coherence. The concepts presented here are extensions of proven techniques that have worked well at synchrotron sources. However, further development will be needed to properly adapt them to the LCLS. **Section 9.4.4** describes the first steps that will be taken along this development path.

## **9.4.2 Facility Diagnostics Instruments**

Each facility diagnostics tanks contains one or more of the following systems:

### **9.4.2.1 Direct Scintillation Imager**

The Direct Scintillation Imager (**Figure 9.18**) is an insertable, high-resolution scintillator viewed by a CCD camera for measuring spatial distributions and for alignment and focusing of optical elements. Traditional instruments have used phosphorus screens to convert x-rays to visible light that can be recorded by a CCD. Even with a microscope objective to magnify the screen, the spatial resolution is limited by the spatial resolution of the phosphorus that is typically

in the range of 10 to 50 microns. Such resolutions are of marginal utility to the LCLS, which has a beam diameter at 8 keV of 100 microns. Recently, workers at the ESRF synchrotron facility have used thin-film single-crystal scintillators for x-rays, achieving 0.8- $\mu\text{m}$  resolution. The scintillator is a 5 micron thick Ce doped YAG crystal on a 100 micron YAG substrate. Other crystals such as LSO are likely to work as well.

The gated-intensified CCD camera can be read out at 120 Hz, providing pulse-to-pulse information.

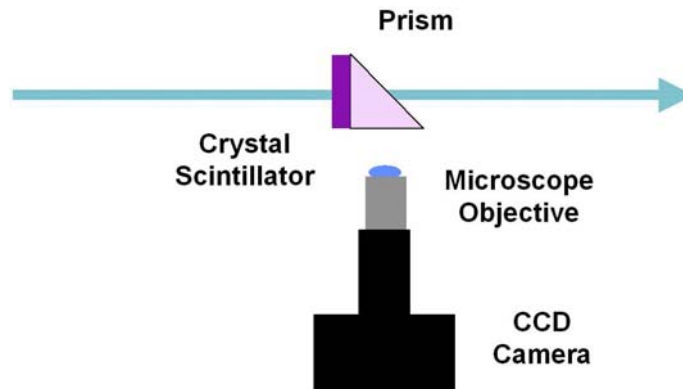


**Figure 9.18** Direct Scintillation Imager

The Direct Scintillation Imager is intrusive – it blocks the beam. Its wide field of view will allow viewing of the spontaneous radiation pattern. In addition, its scintillator is susceptible to damage at the full FEL intensities.

#### 9.4.2.2 Scattering Foil Imager

The Scattering Foil Imager (**Figure 9.19**) overcomes the FEL damage problems of the Direct Scintillation Imager by utilizing a thin foil of a low-Z material such as Be to act as a beam splitter to partially reflect a portion of the beam onto the YAG imaging camera which remains out of the beam. The reflected intensity can be adjusted by changing the angle of incidence. A reflectivity of  $10^{-4}$  can be obtained with an incident angle of  $1^\circ$  at 8 keV and an incident angle of  $>2^\circ$  at 0.8 KeV. Further analysis of this concept is needed to assess the effects of background radiation on the crystal due to Compton scattering of the FEL beam by the Be foil, and of fluorescence from an oxide layer on the foil surface.

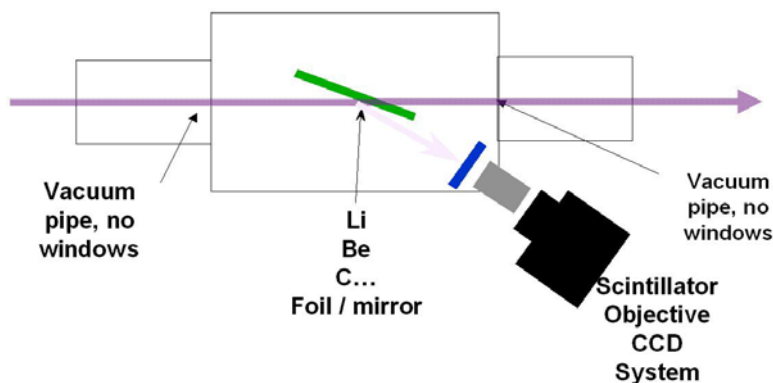


**Figure 9.19** Scattering Foil Imager

With a thin (30 micron) polished Be foil, the Scattering Foil Imager is nearly transparent to the 8 keV radiation and can be used throughout the beam line as a non-intrusive pulse-to-pulse monitor of the beam energy, shape, and centroid. At 0.8 keV, the foil will not be transparent but it will be able to withstand the full FEL intensity, so the Scattering Foil Imager can be used intrusively to measure the pulse-to-pulse statistics of the beam energy, shape, and centroid.

#### 9.4.2.3 Micro-Strip Ion Chamber

The Scattering Foil Imager cannot monitor the 0.8 keV FEL non-intrusively since it is opaque and even at 8 keV it could introduce unwanted distortion into the beam. A traditional ion chamber, commonly used at current synchrotrons, is designed to operate at 1 atmosphere gas pressure, with a fairly low intensity DC beam. The high intensity and pulsed nature of the FEL require some modifications to the traditional design (**Figure 9.20**). The current-measuring electronics of traditional ion chambers must be replaced by pulse processing electronics to measure the energy in each FEL pulse. The drift region must be carefully designed so that the photoelectrons from the pulse are efficiently collected at the anode in the time between pulses. The chamber must be operated at pressures below 1 atmosphere to reduce the instantaneous charge that must be drifted and collected. At 8 keV the gas can be contained within Be windows, but for 0.8 keV operation a windowless chamber with differential pumping is required. Finally low-resolution centroid and shape information can be obtained by segmenting the anode as in a micro-strip detector.

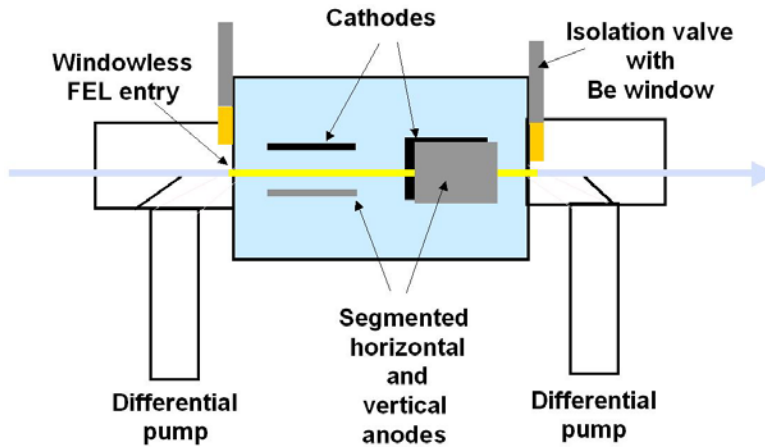


Figure 9.20 LCLS Ion Chamber

Because of the statistical nature of the FEL radiation it is very important to monitor the beam energy, centroid, and overall shape on a pulse-to-pulse basis in a non-intrusive manner. The micro-strip LCLS Ion chamber offers less-intrusive monitoring of the FEL pulse-to-pulse energy as well as low-resolution centroid and shape information. **Figure 9.21** shows the principles of the micro-strip readout.

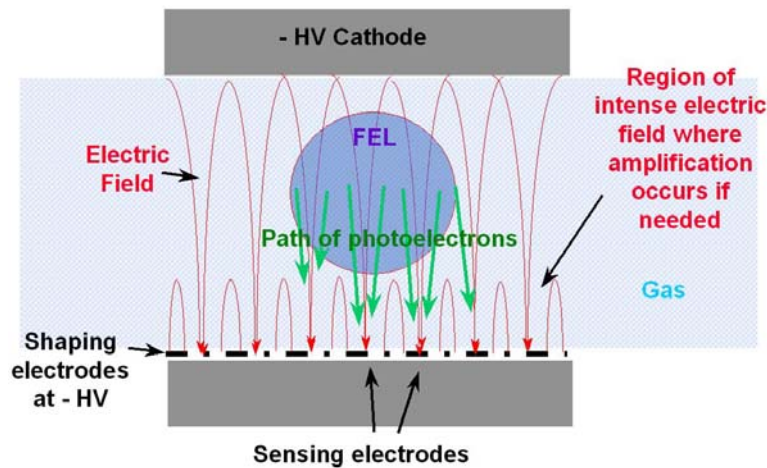
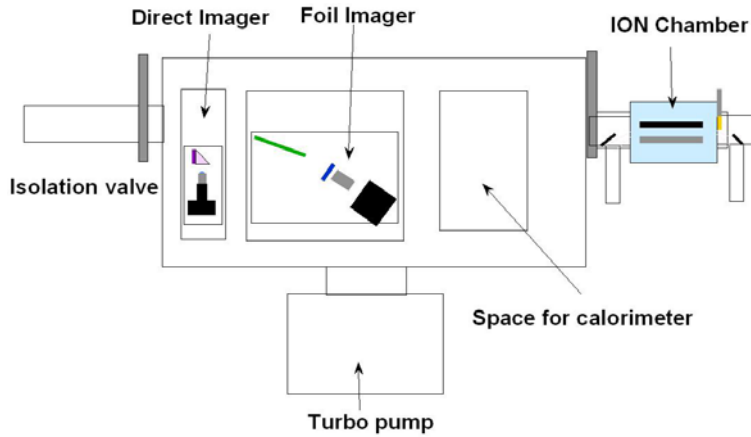


Figure 9.21 Micro-strip Ion Chamber

Photoelectrons liberated by the FEL photons drift down to thin sensing electrodes lithographed onto a substrate. In between the sense electrodes are thicker strips at negative high voltage, which shape the drift field. The centroid and shape are determined by the distribution of charge collected on the sense strips. At sufficient voltage and using correct gas, the electric field in the region near the sense strips can be high enough for gas multiplication to occur. In this regime the sensor is sensitive to single photoelectrons. This could be an advantage for operation at 0.8 keV, since it would then be possible to lower the gas pressure considerably and reduce the pumping load.

### 9.4.2.4 Facility Diagnostic Tanks

The first facility diagnostic tank (FEE 1) is located just downstream of the first set of slits in the FEE (**Figure 9.22**). It contains a Direct Scintillation Imager, a foil imager, and an ion chamber. Since it is the closest diagnostic station to the FEL, and will likely be used heavily during the earliest stages of commissioning, the tank has its own turbo pumping system and is large enough to accommodate other diagnostics.



**Figure 9.22** First Diagnostic Tank (FEE1)

The other diagnostic tanks are similar, though they generally do not have turbo pumps. **Table 9.6** lists the contents of the other facility diagnostics tanks.

**Table 9.6** Diagnostic Tanks

| Tank  | Purpose         | Direct imager | Scattering imager | Ion Chamber | Ion Pump | Turbo pump |
|-------|-----------------|---------------|-------------------|-------------|----------|------------|
| FEE 1 | Slit 1          | X             | X                 | X           | X        | X          |
| FEE 2 | Gas attenuator  | X             |                   |             | X        |            |
| FEE 3 | Wedge + Slit 2  | X             | X                 | X           | X        |            |
| A1 1  | Mirror          | X             | X                 | X           | X        |            |
| A1 2  | (empty)         |               |                   |             |          |            |
| A4 1  | Commissioning   | X             |                   |             | X        | X          |
| B1 1  | Hall B entrance | X             | X                 | X           | X        |            |
| B1 2  | Monochromator   | X             | X                 | X           | X        |            |
| B4 1  | (empty)         |               |                   |             |          |            |

### 9.4.2.5 Ion Chamber Gas Mixing and Distribution System

Micro-strip detectors utilize variants of the so-called “magic gas”, a 3-component mixture of argon, isobutane, and Freon. A gas mixing system, shown schematically in **Figure 9.23**, supplies gas for the micro-strip ion chambers.

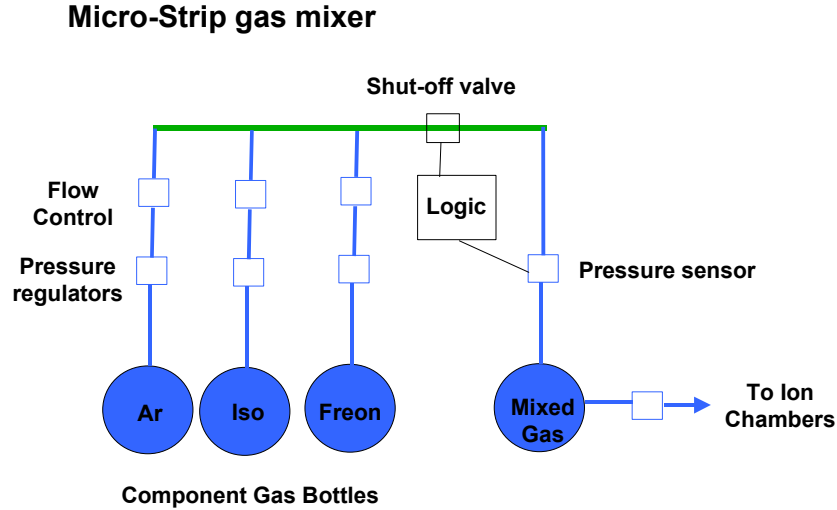


**Figure 9.23** Micro-strip gas mixer

The mixer uses flow controllers to mix the correct amounts of the component gases into a reservoir, which feeds the ion chambers at a slower rate. The mixer logic monitors the reservoir pressure and initiates fill cycles as needed.

### 9.4.3 Commissioning Diagnostics

The intrusive commissioning measurements of total energy, pulse length, spectrum, and transverse coherence will be performed in Hutch A4, tank 1 (**Figure 9.24**). The divergence and spatial shape measurements will be performed using the data from the facility imaging cameras distributed along the beam line.

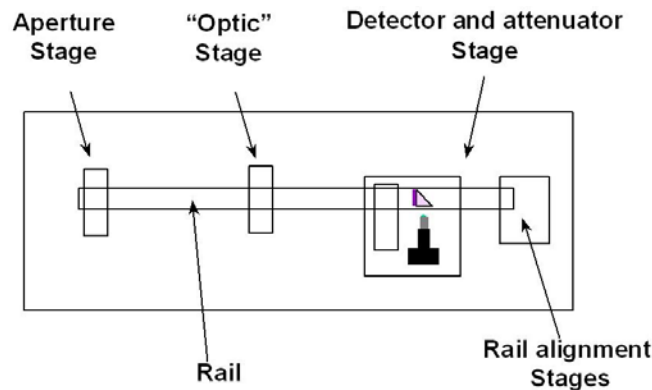


**Figure 9.24** Commissioning Diagnostics tank

The commissioning diagnostic tank has a central optical rail and stages for the necessary apertures, optics, and Direct Scintillation Detector.

### 9.4.3.1 Total Energy

It is desirable to measure the FEL pulse energy utilizing calorimetric techniques to avoid any reliance on the theory of photon-atom interactions at LCLS intensities.

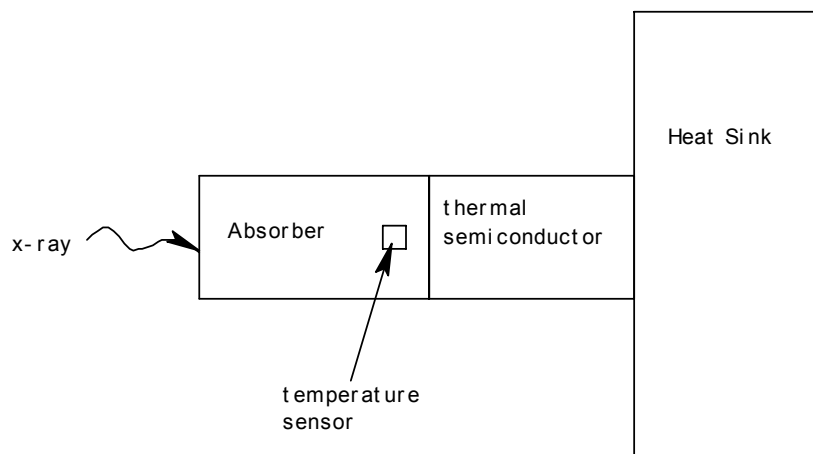


**Figure 9.25** Calorimeter for accurate pulse energy measurement

The calorimeter (**Figure 9.25**) has a small-volume x-ray absorber, which absorbs all of the x-ray energy resulting in a rapid temperature rise dependent on the heat capacity and mass of the absorber. For a 1% measurement, the thickness of the absorber must be at least 5 mean free path lengths in order to capture better than 99% of the x-ray energy. The sensor measures the temperature rise of the absorber. The thermal mass of the sensor is small compared to the absorber. The energy in the absorber is conducted through the thermal weak link to a heat sink held at a constant temperature. The purpose of the thermal weak link is to delay the heat transfer from the absorber to the heat sink long enough to measure the temperature rise in the absorber. The energy deposited by each x-ray pulse is conducted into the heat sink before the arrival of the next x-ray pulse.

For 8 keV operation the absorber could be a Si cylinder 0.5 mm in diameter and 0.5 mm thick. The 0.5 mm thickness is  $> 5$  attenuation lengths and the 0.5 mm diameter nicely accommodates the  $\sim 340$  microns FWHM diameter of the 8 keV FEL at the position of the commissioning diagnostics tank. The dose at 8 keV to Si in this position is 0.12 eV/atom, which is acceptable for a simple absorber.

For 0.8 keV operation the absorber could be a Be disk 3 mm in diameter and  $> 25$  microns thick since the dose to Si at this wavelength is too high. The 3 mm diameter is necessary to contain the 0.88 keV beam whose diameter at this position is 1.9 mm FWHM.

The calorimeter will be positioned on the “optics stage” in the commissioning tank allowing it to be aligned utilizing the rear imaging detector.

### 9.4.3.2 Pulse Length

Measuring the 233 fs pulse length is perhaps the most challenging measurement at the LCLS. Several concepts have been proposed, all involving a medium, which modulates an external laser beam when exposed to the x-ray FEL. **Figure 9.26** illustrates one possible method. The beam from a 1500-nm CW laser is split and made to pass through the two arms of an interferometer patterned in GaAs on a substrate. x-rays impinging on one of the arms changes its index of refraction, causing a modulation in the laser beam after it is recombined. The modulation of the laser beam is in principle of the same duration as the x-ray pulse and can be measured with a streak camera with an accuracy of about 0.5 ps. To achieve better temporal resolution, the modulated optical laser beam is sent through a “time microscope” which stretches the pulse by a factor of  $2\times$  to  $100\times$ . The stretched pulse length is then measured with the streak camera.

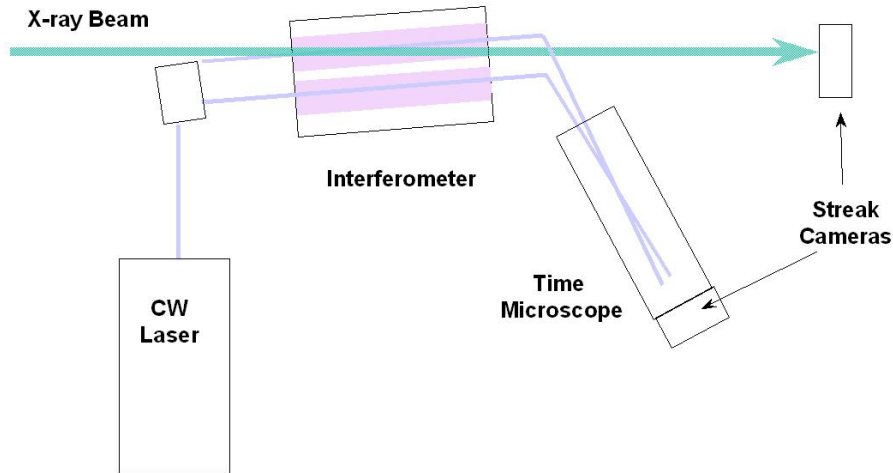


**Figure 9.26** Pulse length measurement

The device can also be used to synchronize an external laser pulse with the x-ray beam. This is accomplished by feeding the external pulse through the time microscope alongside of the x-ray modulated CW pulse and measuring both on the same streak camera.

### 9.4.3.3 Photon Spectrum

The commissioning diagnostic tank is converted into a spectrometer (**Figure 9.27**) by adding a crystal at 8 keV or a grating at 0.8 keV. In either case the optic disperses the radiation onto the x-ray sensitive region of a fast readout position-sensitive detector.

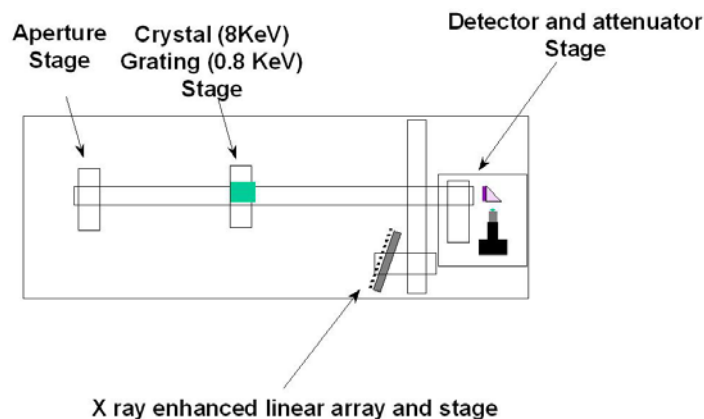


Figure 9.27 Spectrum measurement

#### 9.4.3.4 Transverse Coherence

The transverse coherence could be measured in the commissioning diagnostics tank using the setup shown in **Figure 9.28**, which employs an array of double slits with constant slit width but different slit spacing. The slits sample the beam in two places and the resulting diffracted beams interfere with each other at the position of the detector.

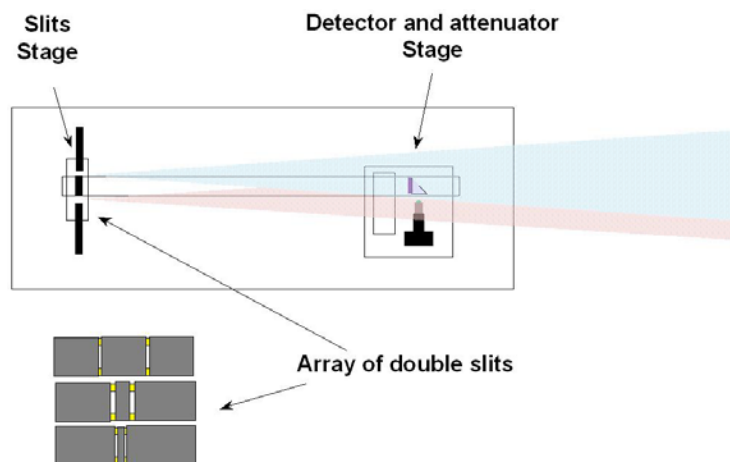


Figure 9.28 Spatial coherence measurement

At 0.8 keV the slits will be assembled from polished sticks of low-Z material such as  $B_4C$  or Si, held apart by spacers. The higher resolution “slits” for 8 keV will be manufactured by the sputter-slice method or from an array of fibers.

#### 9.4.3.5 Spatial Shape and Centroid Location

The spatial shape and centroid location of the FEL beam will be measured on a pulse-by-pulse basis by the Scattering Foil Detectors located in the facility diagnostics tanks distributed along the beam lines.

### 9.4.3.6 Divergence

This measurement is performed at 8 keV using the Scattering Foil Detectors located along the beam line. The measurement is performed at 0.8 keV using the LCLS Segmented Ion Chambers located along the beam line.

### 9.4.4 Diagnostics Modeling

The predictions of the properties of the LCLS FEL beam raise many concerns in the design of the diagnostics, including short pulse effects, power loading, Compton backgrounds, spontaneous background, effects of higher harmonics, and effects due to the coherence of the beam — to name a few. A detailed understanding of these effects is critical for the successful design of each of the diagnostics. This section describes the simulation efforts needed for each diagnostic in order to make efficient use of codes common to all.

A “wave” model will be assembled to propagate the FEL radiation through the diagnostic instrumentation. Ginger simulations will provide the initial FEL radiation characteristics. The code breaks the Ginger FEL beam into its Gauss-Hermite components and contains modules for calculating the action of mirrors, crystals, apertures, multilayers, and zone plates on each of the modes. By summing the modified modes, the code will produce a quantitative image of the time history of the electromagnetic field at the diagnostic and maps of the power loading on each component.

Also, a Monte-Carlo model will be assembled to quantify efficiencies and backgrounds. The Monte-Carlo code generates photons according to the electromagnetic field distributions produced by the wave model as well as spontaneous photons. It tracks the photons through the diagnostic materials (gas, scintillator, etc.), generating Compton and photoelectrons according to the photon cross sections.

Both wave and Monte-Carlo simulations will be performed for each diagnostic.

## 9.5 References

- 1 R. Tatchyn, et al., "X-Ray Optics Design Studies for the 1.5-15 Å LCLS at SLAC", in *Coherent Electron-Beam X-Ray Sources: Techniques and Applications*, A.K. Freund, H.P. Freund, and M.R. Howells, eds., SPIE vol. 3154 (1997).
- 2 B. Adams, personal communication; P. Bucksbaum, personal communication.
- 3 R. M. Bionta, “Controlling Dose to Low Z Solids at LCLS”, LCLS note LCLS-TN-00-3
- 4 R. Tatchyn, "LCLS Optics: Technological Issues and Scientific Opportunities," in *Proceedings of the Workshop on Scientific Applications of Short Wavelength Coherent Light Sources*, SLAC Report 414; SLAC-PUB 6064, March 1993
- 5 R. Tatchyn, P. Csonka, H. Kilic, H. Watanabe, A. Fuller, M. Beck, A. Toor, J. Underwood, and R. Catura, "Focusing of undulator light at SPEAR with a lacquer-coated mirror to power densities of  $10^9$  watts/cm<sup>2</sup>," SPIE Proceedings No. 733, 368-376(1986)

- 6 D. Ryotov and A. Toor, "x-ray attenuation cell", LCLS TN-00-10 (2000)
- 7 D. R. Walz, A. McFarlane, E. Lewandowsky, J. Zabdyr, "Momentum Slits, Collimators, and Masks in the SLC," Proceedings IEEE 1989 Particle Accelerator Conference, IEEE Catalog # 89CH2669-0, 553(1989); SLAC-PUB 4965
- 8 R. Tatchyn, G. Materlik, A. Freund, J. Arthur, eds., Proceedings of the SLAC/DESY International Workshop on the Interactions of Intense Sub-Picosecond X-Ray Pulses with Matter, SLAC, Stanford, CA, Jan. 23-24, 1997; SLAC-WP-12.
- 9 S. Dushman, *Scientific Foundations of Vacuum Technique*, John Wiley, New York, 1941.
- 10 H. N. Chapman, et al., *J. Vacuum Sci. Technol.* **B19**, 2389 (2001)
- 11 G.E. Ice, J.-S. Chung, J. Z. Tischler, A. Lunt, and L. Assoufid, *Rev. Sci. Instrum.* **71**, 2635 (2000).
- 12 A. Freund, "Crystal Optics for the LCLS," presented at the SLAC/DESY International Workshop on the Interactions of Intense Sub-Picosecond X-Ray Pulses with Matter, SLAC, Stanford, CA, Jan. 23-24, 1997.
- 13 Differential Pump DP-01, XHA X-Ray Instrumentation Associates, Mountain View, CA 94043.